Catalysis Today 172 (2011) 111–117

Contents lists available at ScienceDirect

Catalysis Today

journal homepage: www.elsevier.com/locate/cattod

Catalytic performance in methane combustion of rare-earth perovskites $RECo_{0.50}Mn_{0.50}O_3$ (RE: La, Er, Y)

Gina Pecchi[a], Claudia Campos[a,b], Octavio Peña[b,*]

[a] Facultad Ciencias Químicas, Universidad Concepción, Casilla 160-C, Concepción, Chile
[b] Sciences Chimiques de Rennes, UMR 6226, CNRS, Université de Rennes 1, Rennes, France

ARTICLE INFO

Article history:
Received 25 November 2010
Received in revised form 6 February 2011
Accepted 14 February 2011
Available online 31 March 2011

Keywords:
Perovskites
Methane
Combustion
Erbium
Yttrium
Lanthanum

ABSTRACT

$RECo_{0.50}Mn_{0.50}O_3$ perovskites (RE: La, Y, Er) have been prepared by an auto-combustion method and calcined at 700 °C, 850 °C and 950 °C. $YCo_{0.50}Mn_{0.50}O_3$ forms at temperatures as low as 700 °C, much lower than those required in solid-state ceramic synthesis. All materials show adequate specific surface when calcined at 700 °C. $ErCo_{0.50}Mn_{0.50}O_3$, which has the largest surface area, shows the lowest activity due to the presence of segregated phases, while $YCo_{0.50}Mn_{0.50}O_3$, which reaches the perovskite structure at lower temperatures, exhibits the highest catalytic activity. The catalytic activity, evaluated from the total combustion of methane, can be related to the presence of the perovskite structure, an adequate surface area and the reducibility of the material. At the calcination temperatures of 850 °C and 950 °C, at which the surface area and crystalline degrees are almost the same for the La-, Y- and Er-systems, no differences in the catalytic activity were detected. The catalytic activity, higher for materials calcined at lower temperatures, is progressively lost due to sintering processes occurring at higher calcinations temperatures, as confirmed by SEM observations.

1. Introduction

Mixed valence perovskites ABO_3 have been studied in the last 20 years because of their exceptional properties, in particular existence of a magnetoresistance phenomenon due to a double mechanism of exchange interactions and presence of mobile electrons, leading to a metal-insulator transition coupled to a ferromagnetic ordering [1,2]. Most of the reports concern the substitution of the rare-earth RE cation located at the A-site by alkaline-earth elements since, by this way, the Mn^{3+} ion at the B-site transforms into Mn^{4+}, triggering double-exchange interactions through the oxygen orbitals [3]. Less known are the substitutions at the B-site, for which, similar mechanisms occur provided the manganese ion is substituted by a divalent transition-metal element, such as Ni, Co or Cu [4]. The case of the cobalt ion is especially interesting since cobalt may adopt a 2+ or 3+ oxidation state, depending upon the synthesis conditions and the substitution rate [5]. Based on the equilibrium relation $RE^{3+}Co^{2+}{}_{0.50}Mn^{4+}{}_{0.50}O_3$, a charge and nuclear orderings are expected at the equiatomic content Co/Mn = 0.5/0.5, for which all Mn ions are converted into Mn^{4+}, triggering strong ferromagnetic Co^{2+}–Mn^{4+} interactions, large coercive fields H_{coerc} and a maximum value of the ordering temperature T_c [6,7]. The nature and size of the rare-earth cation plays also a role on fixing the physico-chemical properties of the ensemble [8]. Small-size ions like Y or Er, lead to large structural distortions imposed by the ionic radius at the A-site, independent whether the cation is magnetic (Er) or not (Y).

In previous studies we have reported the magnetic, catalytic and thermal stability in reductor atmosphere of the solid solution $LaCo_xMn_{1-x}O_3$ ($0.0 \leq x \leq 1.0$). In particular, we found that the intrinsic catalytic activity and the reaction rate altogether with the ferromagnetic parameters (paramagnetic Curie–Weiss Θ and transition T_c temperatures) attain maximum values at the equimolar composition $LaMn_{0.50}Co_{0.50}O_3$ [9,10]. Presence of Mn and Co ions in equimolar quantities stabilizes the crystalline structure (orthorhombic at $x < 0.5$) and rhombohedral at $x > 0.5$) and eventually leads to a cationic ordering of Mn and Co atoms. These interesting magnetic, catalytic and thermodynamic properties observed at the equimolar composition $LaMn_{0.50}Co_{0.50}O_3$ made us to extend its study, modifying the nature of the RE cation. In this work we present the influence of the RE cation on the physico-chemical properties of the equimolar perovskites $REMn_{0.50}Co_{0.50}O_3$. Replacing La by Er or Y, both ions having a much smaller ionic radius than the one for La, modifies the microstructural properties and the interatomic distances and angles, leading to weaker magnetic interactions and a much lower transition temperature. In addition, Y (no 4f shell) and Er ($4f^{11}$) have quite different magnetic properties (0 and 9.58 μ_B, respectively), so important modifications are expected with respect to the nature of

* Corresponding author.
E-mail address: octavio.pena@univ-rennes1.fr (O. Peña).

0920-5861/$ – see front matter © 2011 Elsevier B.V. All rights reserved.
doi:10.1016/j.cattod.2011.02.032

the phases formed, their crystalline degree, purity and composition and in the electronic modifications which could have consequences in the oxygen stoichiometry and on the catalytic activity.

2. Experimental

2.1. Preparation

The $RECo_{0.50}Mn_{0.50}O_3$ (RE: La, Er, Y) perovskites were prepared by the solution combustion synthesis (SCS) using the glycine–nitrate process [11]. The used reactants were: $La(NO_3)_3{\cdot}6H_2O$ (Merck,99%), $Mn(NO_3)_2{\cdot}4H_2O$(Merck), $Co(NO_3)_2{\cdot}6H_2O$ (Merck), Er_2O_3 (Aldrich), erbium nitrate was prepared using nitric acid (65%p/p, 1.392 g mL^{-1}), $Y(NO_3)_3{\cdot}6H_2O$ (Aldrich) and glycine (NH_2CH_2COOH) (Aldrich) used as sacrificial fuel. The preparation was carried out combining glycine with the metal nitrates in stoichiometric ratios in aqueous solution. The precursor was heated to evaporate excess water, yielding a viscous liquid. Further heating to about 180 °C caused the precursor liquid to autoignite. Combustion was rapid and self-sustaining, with flame temperatures reaching values far above 1100 °C [11]. The prepared solids were crushed and sieved to obtain the required particle size (<200 μm) prior to calcination at 400 °C in air for 2 h to eliminate the organic components. The effect of the calcination temperatures was studied at 700 °C, 850 °C and 950 °C in air for 3 h.

2.2. Characterization

X-ray powder diffraction patterns of all calcined samples were obtained with nickel-filtered Cu-$K\alpha_1$ radiation ($\lambda = 0.15418$ nm) using a Rigaku diffractometer. Phase identification was carried out by comparison with the JCPDS-ICDD database cards ($LaMnO_3$ JCPDS 32-0484, $LaCoO_3$ JCPDS 84-0848, $YMnO_3$ JCPDS 25-1079, $YCoO_3$ JCPDS 88-0425, $ErMnO_3$ JCPDS 14-0689, $ErCoO_3$ JCPDS 73-1197) and confirmed the presence of the perovskite reflections. Specific areas were calculated using the BET method from the nitrogen adsorption isotherms, recorded at 77 K on a Micromeritics apparatus Model ASAP 2010 in the 0.05–0.995 relative pressure range, taking a value of 0.162 nm^2 for the cross-sectional area of the adsorbed N_2 molecule (AGA, 99.995%). Prior to the adsorption measurements, samples were outgassed at 150 °C. Temperature-programmed reduction (TPR) experiments were performed in a TPR/TPD 2900 Micromeritics system equipped with a thermal conductivity detector. Samples of about 20 mg were placed in a U-shape quartz tube, first purged in a synthetic air stream of 50 mL min^{-1} at 500 °C for 1 h and then cooled to ambient temperature. Reduction profiles were then recorded by passing a 5% H_2/Ar flow (both gases from AGA, 99.995% purity) at a rate of 40 mL min^{-1} while heating at a rate of 10 °C min^{-1} from ambient temperature to 900 °C. A cold-trap was placed just before the thermal conductor detector (TCD) of the instrument to remove the water from the exit stream. For the oxygen desorption O_2-TPD experiments, the samples were exposed to oxygen (AGA 99.5%) for 1 h at 700 °C, followed by cooling to room temperature in the same atmosphere. After switching the atmosphere to a He (AGA 99.995%) flow, the sample was heated at a constant rate of 10 °C min^{-1} and the desorbed oxygen was monitored with a thermal conductivity detector. Fourier transformed infrared spectra (FTIR) was recorded in a Nicolet Magna-IR 550 instrument, equipped with a quartz sample holder with KBr windows. The perovskites were dehydrated at 210 °C, finely ground in an agate mortar with KBr to obtain a sample/KBr ratio of 1/150. Scanning electron microscopy (SEM) observations and energy dispersion analyses (EDAX) analyses were obtained in a JEOL model JSM 6380 LV.

2.3. Catalytic activity

The studied perovskites were tested in methane combustion using 19,800 mg cm^{-3} of methane, with a total flow rate of 100 mL min^{-1} measured at room temperature and a feed mixture of 2.8 vol% CH_4, 20 vol% O_2 (AGA 99.5%) and 77.2 vol% He (AGA 99.995) as balance in a flow reactor. In each experiment, 0.3 g of catalysts (20–40 mesh) diluted with 1.5 g of SiC, of the same particle size, were loaded into a quartz reactor (inner diameter 1.27 cm) with quartz fiber packed at the end of the catalyst bed. Gas flow rates were carefully adjusted by means of mass flow controllers (Brooks 5850E). Prior to each experiment, the catalyst was treated with 1000 mL min^{-1} (STP) of synthetic air for 1 h at 500 °C. At this temperature, the oxidant gas was switched to the reactant gaseous mixture for 1 h. After that, the sample was cooled down to 300 °C and stabilized for 30 min prior to the catalytic test. The thermocouple was placed inside the reactor just at the beginning of the catalyst bed. The inlet and outlet concentrations of methane and carbon dioxide were analyzed using an on-line gas chromatograph Hewlett Packard model HP 4890D with thermal conductivity detector. Helium was used as a carrier gas and the column used was a 30 m capillary Supelco 25462. The data obtained at each temperature were the average of three steady-state measurements.

3. Results and discussion

3.1. X-ray diffraction

The X-ray diffraction (XRD) of the $RECo_{0.50}Mn_{0.50}O_3$ (RE: La, Er, Y) perovskites as a function of the calcination temperature at 700 °C, 850 °C and 950 °C was performed to identify the crystal structure, its evolution and the crystalline phases developed during the calcination process. To estimate the deviation from the ideal structure, the Goldschmidt tolerance factor t was calculated from the ionic radii of the A and B cations. For the B cation, the average radius of Co and Mn was assumed [12]. The corresponding t values are 0.97, 0.81 and 0.80 for the La-, Y- and Er-perovskites $RECo_{0.50}Mn_{0.50}O_3$, respectively. The t value of 0.97 suggests the presence of cubic or orthorhombic structure, perhaps somewhat distorted for the t values of 0.80 and 0.81.

Fig. 1 displays the diffraction patterns of the studied perovskites for different calcination temperatures. It can be seen that the perovskite structure is obtained in all systems, with peaks increasing in intensity and becoming sharper when increasing the calcination temperature, indicating that the solid progressively becomes pure and well crystallized. Sharp diffraction lines are obtained for $YCo_{0.50}Mn_{0.50}O_3$ at temperatures as low as 700 °C while, for $LaCo_{0.50}Mn_{0.50}O_3$ and $ErCo_{0.50}Mn_{0.50}O_3$, broader diffraction peaks are indicative of a less crystalline solid and that the perovskite structure is more difficult to be formed at 700 °C compared to the case of $YCo_{0.50}Mn_{0.50}O_3$ at equivalent calcination temperatures. A comparison of the XRD data with the JCPDS-ICDD database indicates that all materials prepared in this work belong to the orthorhombic structure.

Even though the perovskite structure may be obtained at low calcination temperatures, presence of other phases in very low concentration, highly dispersed or as amorphous phases cannot be discarded since XRD resolution can be a limiting obstacle. As said above, at higher calcination temperature the solids become well crystallized and any amorphous or spurious phases disappear, as confirmed by the sharper diffraction peaks and from additional experiments, which will be discussed below. The lattice parameters were then determined at the highest calcination temperature (950 °C) and are given in Table 1. As expected, the unit cell volume of the La-based perovskite is much larger than those observed for

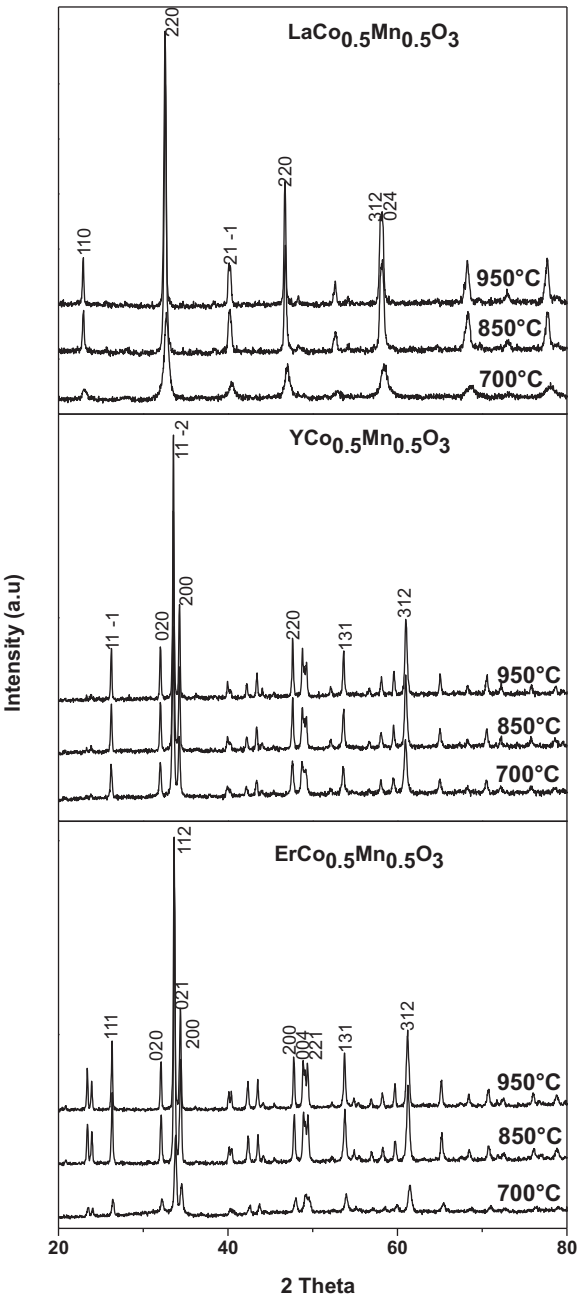

Fig. 1. XRD profiles of $LaCo_{0.50}Mn_{0.50}O_3$, $YCo_{0.50}Mn_{0.50}O_3$ and $ErCo_{0.50}Mn_{0.50}O_3$ calcined at 700 °C, 850 °C and 950 °C.

Table 1
Lattice parameters of the $RECo_{0.5}Mn_{0.5}O_3$, (RE: La, Er, Y) perovskites calcined at 950 °C.

	$a \pm 0.0001$ (nm)	$b \pm 0.0001$ (nm)	$c \pm 0.0001$ (nm)	Volume (nm^3)
$LaMn_{0.50}Co_{0.50}O_3$	0.5534	0.5461	0.7851	0.2372
$YMn_{0.50}Co_{0.50}O_3$	0.5236	0.5582	0.7486	0.2188
$ErMn_{0.50}Co_{0.50}O_3$	0.5212	0.5572	0.7441	0.2161

the Y- and Er-based counterparts due to a bigger ionic radius of the La^{3+} ion ($r_{ion}(La^{3+}) = 1.5$ Å, $r_{ion}(Er^{3+}) = 0.96$ Å, $r_{ion}(Y^{3+}) = 0.93$ Å).

As pointed out above, the size of the lanthanide cation situated at the A-site is one of the main mechanisms of stabilization of the structure since it imposes a lattice distortion and modifies the interaction mechanism, which takes place along the Mn^{4+}—O—Co^{2+} bonding. This has a direct incidence on the crystal's symmetry besides strong modifications of the strength of the ferromagnetic interactions. It is not surprising then that $YCo_{0.50}Mn_{0.50}O_3$ and $ErCo_{0.50}Mn_{0.50}O_3$, with Er^{3+} and Y^{3+} at the RE position, present the same symmetry. A characteristic triplet for the Y and Er systems appears at 2θ values between 30° and 35°. The larger La^{3+} cation exhibits an orthorhombic structure with higher symmetry. Table 2 shows the average particle size d, assuming that particles are spherical, determined according to Scherrer's formula ($d = 0.9\lambda/B\cos\theta$), where λ is the wavelength of the Cu-Kα radiation, B the full width at half maximum of the diffracted peak and θ the Bragg diffraction angle. As expected, an increase with calcination temperature can be observed, indicating a tendency to form large grain and more crystalline perovskites.

3.2. Fourier transformed infrared spectroscopy

Infrared (IR) spectra are presented in Fig. 2. The most important band of the perovskite structure, ν_1, corresponding to the asymmetrical lengthening of the B—O bond of the BO_6 octahedrons [13], is observed at 604 cm^{-1}, although it presents some differences in intensity as a function of the nature of the RE cation and the calcination temperature. Almost no differences in the ν_1 band for the $LaCo_{0.50}Mn_{0.5}O_3$ and $YCo_{0.50}Mn_{0.5}O_3$ upon calcination temperatures can be detected, while for $ErCo_{0.50}Mn_{0.50}O_3$, the ν_1 band appears at 850 °C, becoming sharper at 950 °C. The absence of ν_1 band for $ErCo_{0.50}Mn_{0.50}O_3$ sample calcined at 700 °C, indicates that this sample, at least in a slight extent, presents a mixture of oxides and a poor perovskite structure. The broad band at 3200 cm^{-1} and the small one at 1500 cm^{-1}, are assigned to the lengthening of the water O—H bond ν_{O-H} and δ_{H-O-H} due to the exposure of the perovskites to air and environmental humidity. The $ErCo_{0.50}Mn_{0.50}O_3$ system also presents a small band at 2800 cm^{-1} assigned to carbonated phases, and weak bands at 1495 cm^{-1} and 1377 cm^{-1}, corresponding to the vibration mode ν_3 of the CO_3^{2-} groups associated to the presence of segregated phases in the form of carbonates. The low extent of carbonation and the absence of diffraction lines associated to segregated oxide phases are in agreement with our XRD data, since if segregated oxides are present, they must be in a high dispersion degree.

3.3. SEM

The particle size and morphology of the calcined powders were examined by scanning electron microscopy (SEM). Fig. 3 shows SEM images of the perovskites calcinated at 700 °C, 850 °C and 950 °C. The images indicate that the synthesis favours the formation of a fine powder with uniform grain distribution and homogeneous nanostructure, with mean values for the grains' size in the nanoscale range, between 20 and 100 nm. The decrease of the particle size with doping is mainly due to two reasons: (i) differences

Table 2
Crystallite size evaluated by XRD and SEM and specific surface area for $RECo_{0.50}Mn_{0.50}O_3$ (RE: La, Er, Y) perovskites.

	d (nm) XRD			d (nm) SEM			S_{BET} (m^2g^{-1})		
	700 °C	850 °C	950 °C	700 °C	850 °C	950 °C	700 °C	850 °C	950 °C
$LaMn_{0.50}Co_{0.50}O_3$	40	45	45	40	80	120	22	11	8
$YMn_{0.50}Co_{0.50}O_3$	26	52	52	50	75	100	23	11	7
$ErMn_{0.50}Co_{0.50}O_3$	29	45	45	45	75	140	36	14	8

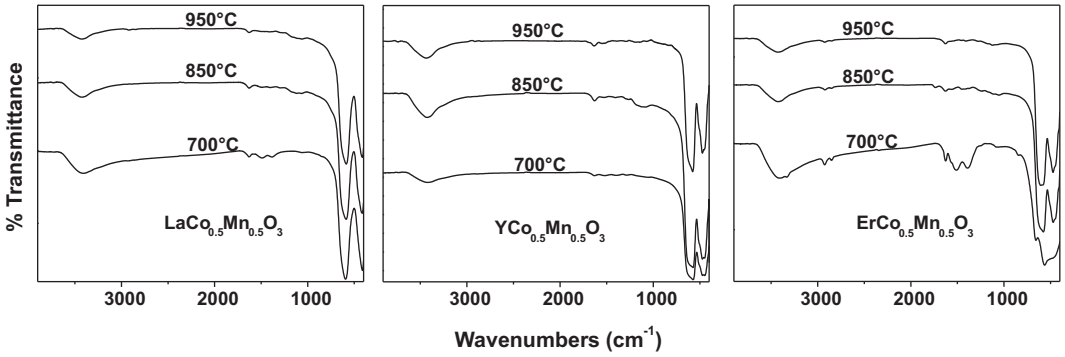

Fig. 2. FTIR of $LaCo_{0.50}Mn_{0.50}O_3$, $YCo_{0.50}Mn_{0.50}O_3$ and $ErCo_{0.50}Mn_{0.50}O_3$ calcined at 700 °C, 850 °C and 950 °C.

between the ionic radii of the dopant atom with that of actual site atom, and (ii) increasing the density of defects due to doping [14]. Upon sintering at 850 °C and 950 °C, the grain distribution becomes more homogeneous, showing a strong similarity for the three studied systems. A very good percolation is achieved at about 950 °C with respect to calcination at 700 °C and 850 °C. The mean particle size evaluated from the SEM images changes with the same trend as observed from the X-ray diffraction data, as shown in Table 2. It can be seen that the grain size determined by the XRD peak broadening differs from the one determined from SEM. This is because the latter includes the grain boundary region, while Scherrer's formula gives the crystallite size (i.e., length of coherence) in a direction perpendicular to the incident X-ray beam.

3.4. Specific surface area

Table 2 shows the dependence of the corresponding BET specific surface areas (S_{BET}) with calcination temperatures. As expected, a decrease in the S_{BET} values upon calcination can be detected. An almost linear dependence of S_{BET} with the calcination temperature can be observed for $LaCo_{0.50}Mn_{0.50}O_3$ and $YCo_{0.50}Mn_{0.50}O_3$, whereas for the Er system a large surface area was obtained for the material calcined at 700 °C, reaching almost the same S_{BET} values as the Y- and La-systems when calcined at 850 °C and 950 °C. From the XRD and FTIR results, the higher specific area of the Er-system can be attributed to mixed oxides in a high dispersion degree. Since the specific surface values and the crystalline degree are properties

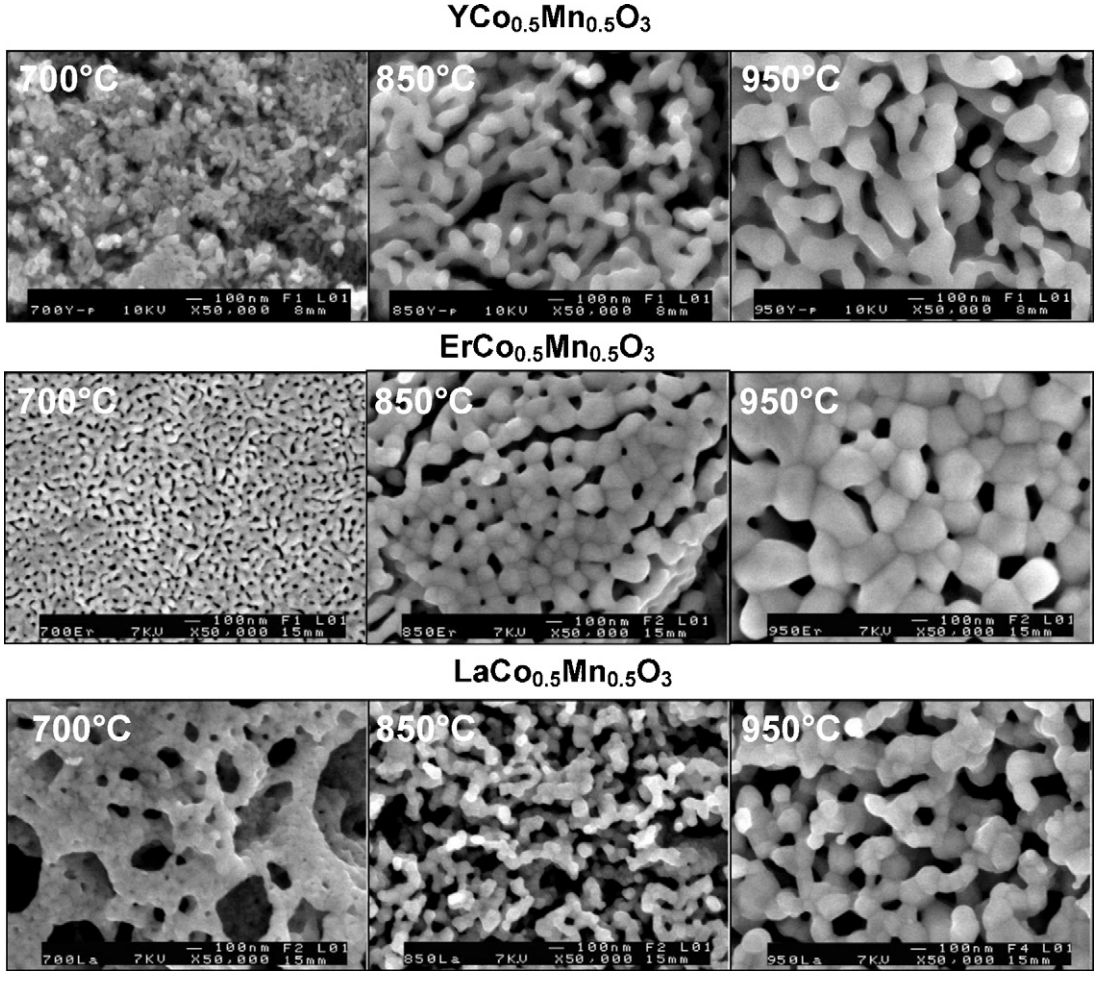

Fig. 3. SEM micrographs of $LaCo_{0.50}Mn_{0.50}O_3$, $YCo_{0.50}Mn_{0.50}O_3$ and $ErCo_{0.50}Mn_{0.50}O_3$ calcined at 700 °C, 850 °C and 950 °C.

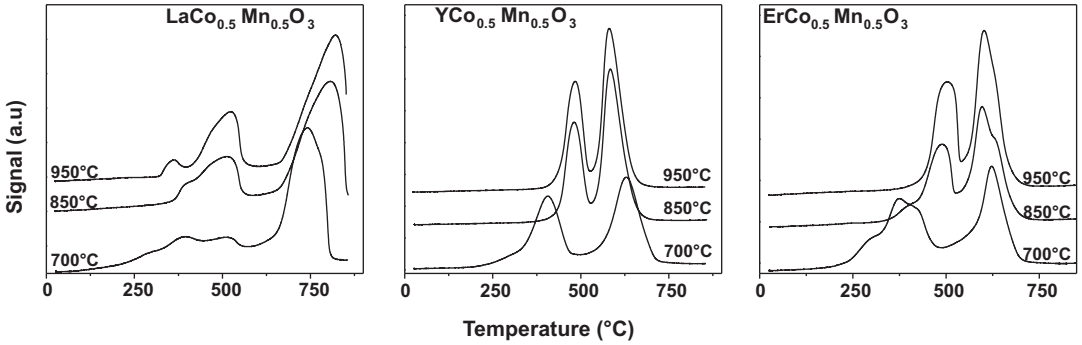

Fig. 4. Temperature-programmed reduction of $LaCo_{0.50}Mn_{0.50}O_3$, $YCo_{0.50}Mn_{0.50}O_3$ and $ErCo_{0.50}Mn_{0.50}O_3$ calcined at 700 °C, 850 °C and 950 °C.

that vary inversely proportional, it is expected that the lowest S_{BET} values must be obtained in perovskites with the highest mean particle size, as observed by SEM and XRD. Considering the obtained XRD, SEM and S_{BET} results, a good correlation between these two properties is obtained.

3.5. Temperature profile reduction

To study the thermal stability in reducing atmosphere, a reduction step under H_2/Ar flow up to 900 °C was carried out after the calcination steps. The TPR profiles are shown in Fig. 4. Two reduction steps can be seen, with differences in shape, intensity and temperature. The TPR profiles for $LaCo_{0.50}Mn_{0.50}O_3$ show a broad and not well-defined first reduction peak at low temperatures followed by an intense reduction peak at higher temperature. The similarity of the TPR profiles of the $LaCo_{0.50}Mn_{0.50}O_3$ calcined at 700 °C, 850 °C and 950 °C indicates a similar chemical composition and crystalline structure, and the effect of the calcination temperature is only to increase crystallinity. The first reduction step can be attributed to the loss of lattice oxygen to form an oxygen-deficient perovskite structure, as it has been pointed out for this type of oxides [15]. As La^{3+} is a non-reducible ion, the second reduction peak can be interpreted as the Mn^{4+} reduction of the Mn^{4+}–Co^{2+} network to yield $La_2Mn_2O_5$ [16] and/or $La_2Co_4O_6$ as intermediate reduction products [17]. The complete reduction of the perovskite structure occurs between 600 °C and 850 °C with formation of La_2O_3, $La(OH)_3$, MnO, CoO, Co^0 and H_2O [18]. $YCo_{0.50}Mn_{0.50}O_3$ shows different reduction profile compared to the one just described, with two symmetric and well-defined reduction peaks independent of the calcination temperature. This reduction profile is indicative of the absence of multiple phases and confirms that for Y-system, a homogeneous chemical composition is obtained. The first peak at 400 °C also corresponds to the formation of oxygen-deficient perovskite structures, and the second one to the complete reduction of the perovskite structure with formation of Y_2O_3, MnO, CoO and Co^0, as previously reported [9]. The shift towards lower temperatures of the first reduction peak of the $YCo_{0.50}Mn_{0.50}O_3$ perovskite calcined at 700 °C can be explained considering the XRD results: a less crystalline structure is easier to reduce. Again, the similarity of the TPR profiles for the $YCo_{0.5}Mn_{0.5}O_3$ samples calcined at 850 °C and 950 °C confirms their similar structure and chemical composition. The shift of the second reduction peaks towards lower temperatures when the sample is calcined at 850 °C and 950 °C is in agreement with the sintering process due to the increase in the diffusional resistance of the solids.

Comparing the nature of the RE cation, at 700 °C the first reduction peak of the La- and Er-systems is broader with shoulders indicative of the presence of more than one type of bulk oxides as segregated phases. On the contrary, the Y-system presents a well-defined first reduction peak. Therefore, the formation of an oxygen-deficient perovskite structure occurs much cleaner and in a large extent for the Y-system. Concerning the $ErCo_{0.50}Mn_{0.50}O_3$ system, the not well-defined peaks for the samples at 700 °C is a consequence of the reduction of the multiple phases present in varying concentration in the mixed oxides. Increasing the calcination temperature shows better defined peaks and favours an isomorphic transition of the segregated oxide, which transforms into the crystalline perovskite structure forming a pure phase. The broad reduction peak can be related to the poor crystallization of the sample, in which these lower coordination oxides are reducible at lower temperatures than the oxides of perovskite structure.

3.6. Oxygen desorption profile

The evolution of oxygen during temperature-programmed desorption (TPD) experiments provides information dealing with the redox properties of these oxides [19]. The O_2-TPD profiles are shown in Fig. 5. Three desorption peaks have been reported for perovskite-type oxides: (i) physisorbed oxygen species, O^-_2(ads), at temperatures below 150 °C assigned to ordinary chemically

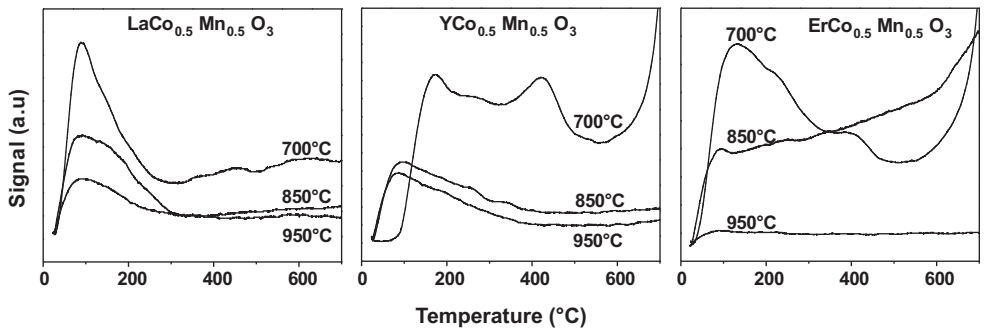

Fig. 5. Oxygen desorption profiles of $LaCo_{0.50}Mn_{0.50}O_3$, $YCo_{0.50}Mn_{0.50}O_3$ and $ErCo_{0.50}Mn_{0.50}O_3$ calcined at 700 °C, 850 °C and 950 °C.

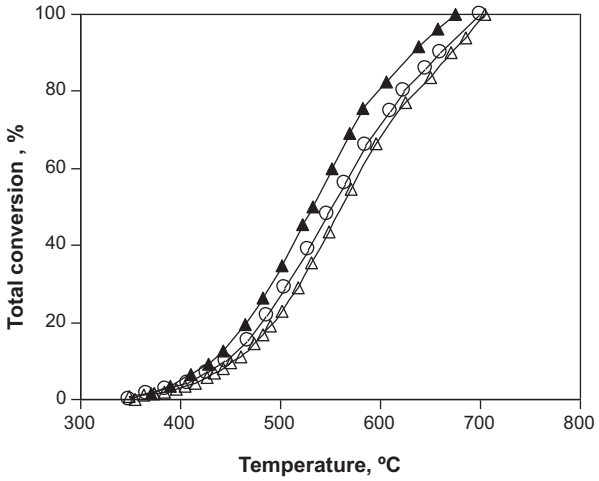

Fig. 6. Stationary-state conversion of: (Δ) $LaCo_{0.50}Mn_{0.50}O_3$; (○) $YCo_{0.50}Mn_{0.50}O_3$; (▲) $ErCo_{0.50}Mn_{0.50}O_3$, calcined at 850 °C.

adsorbed oxygen, i.e., surface hydroxyls, (ii) α-oxygen species, O^-, at temperatures between 200 °C and 400 °C assigned to species adsorbed to the surface oxygen vacancies; (iii) β-oxygen species, O^{2-}, at temperatures higher than 500 °C associated with oxygen species occupying the inner vacancies of the lattice [20]. The expected trend for $LaCo_{0.50}Mn_{0.50}O_3$ perovskites is observed, as shown in Fig. 5. For the perovskite calcinated at 700 °C physisorbed species and α-oxygen are observed, while a large desorption peak starts to appear at high temperatures although not fully finished. TPD–Mass Spectroscopy experiments confirm that the evolved gas and the He flow only contain oxygen. For the perovskites calcinated at 850 °C and 950 °C, only physisorbed species are present due to their low S_{BET} and high crystalline degree. As expected, the Y-system calcinated at 850 °C and 950 °C presents almost identical desorption profiles. A different behaviour is detected for the $YCo_{0.50}Mn_{0.50}O_3$ calcinated at 700 °C, which presents physisorbed species, a large extent of α-oxygen and β-oxygen, this latter represented by the large peak starting at 550 °C and not finished at 700 °C. Even though, the 700 °C-$ErCo_{0.50}Mn_{0.50}O_3$ shows similar oxygen desorption profile, the lower extent of α-oxygen is a consequence of the low percentage of the perovskite structure present in this solid. For a material calcined at 850 °C and 950 °C, the perovskite structure is favoured and, as a consequence, a lower surface area and a low extent of desorbed oxygen was observed.

Table 3
Ignition temperature (T_{ign}^{50}) in methane combustion on $RECo_{0.50}Mn_{0.50}O_3$ (RE: La, Er, Y) perovskites.

	T_{ign}^{50} (°C)		
	700 °C	850 °C	950 °C
$LaMn_{0.50}Co_{0.50}O_3$	475	562	635
$YMn_{0.50}Co_{0.50}O_3$	510	552	629
$ErMn_{0.50}Co_{0.50}O_3$	480	533	635

3.7. Catalytic activity

Fig. 6 shows the activity data for methane oxidation as a function of the reaction temperature up to complete combustion for the solids calcined at 850 °C. Typical sigmoidal curves can be seen in which the reaction starts at about 350 °C, then the conversion increases drastically as the temperature increases until complete conversion. A shift towards higher temperatures indicates lower activity. Carbon dioxide and water were the only observed products of the reaction. Differences in the conversion level at a given temperature for the perovskites having different RE cation and calcination temperature were observed. The ignition temperature (T_{ign}^{50}), defined as the temperature required to obtain 50% of methane conversion is compiled in Table 3. A subsequent increase in T_{ign}^{50}, i.e., a decrease in the catalytic activity upon calcination temperature, is observed. The low T_{ign}^{50} of the 700 °C-$LaMn_{0.50}Co_{0.50}O_3$ can be related with the higher α-oxygen desorption temperature for the less electronegative rare-earth metals [21]. Considering that the reported T_{ign}^{50} for total combustion of methane carried out over various partially cation-substituted La–Fe, La–Mn, and La–Co perovskite-type oxides are in the range 525–780 °C [22], the decrease of T_{ign}^{50} for the studied $RECo_{0.50}Mn_{0.50}O_3$ perovskites calcined at 700 °C is quite remarkable. The specific activity (expressed as mol converted per second and per gram of catalyst) and the intrinsic activity (expressed as mol converted per second and per square-meter of catalyst) evaluated at 420 °C and conversion level <10% are shown in Fig. 7a and b, respectively. It can be seen that the specific and intrinsic reaction rates show the same trend, the highest catalytic activities being those of the catalysts calcined at 700 °C and the lowest to those calcined at 950 °C. For calcination temperatures of 850 °C and 950 °C, the samples exhibit almost the same reaction rate and thermal behaviour in agreement with the crystallochemical characterisation, that is, similar structure and specific area. Larger differences in the catalytic behaviour are obtained for the perovskites calcined

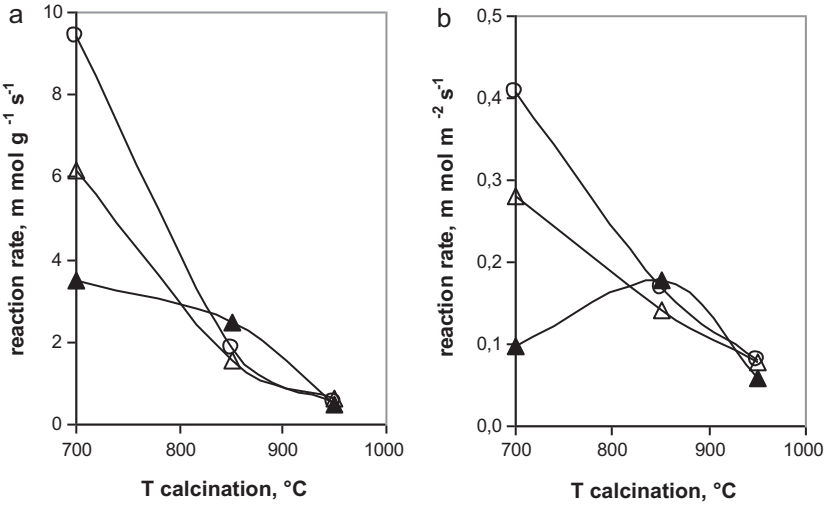

Fig. 7. (a) Specific and (b) intrinsic activity evaluated at 420 °C as a function of calcination temperature of: (Δ) $LaCo_{0.50}Mn_{0.50}O_3$; (○) $YCo_{0.50}Mn_{0.50}O_3$ and (▲) $ErCo_{0.50}Mn_{0.50}O_3$.

at 700 °C, which can be explained considering the results discussed previously. The large reaction rate of $YCo_{0.50}Mn_{0.50}O_3$ calcined at 700 °C is attributed to its larger crystalline degree, presence of α-oxygen and an adequate surface area compared to the other perovskites. Even though the $LaCo_{0.50}Mn_{0.50}O_3$ perovskite calcined at 700 °C has the same S_{BET} value (Table 2), its low reaction rate can be attributed to a less crystalline structure obtained at 700 °C. For the $ErCo_{0.50}Mn_{0.50}O_3$ perovskite calcined at 700 °C, which exhibits the largest S_{BET} value, its low reaction rate is attributed to a low content of the perovskite compound plus the presence of segregated phases.

Therefore the nature of the RE cation and the calcination temperature produce a modification of the active sites required for catalytic reactions at 700 °C. On the contrary, the differences in the crystalline degree, nature of phases, nature of oxygen, among others, which were clearly observed in samples after calcination at 700 °C, were not observed at 850 °C and 950 °C due to the high temperature of calcination. Therefore, the reaction rate in the total combustion of methane can be closely related to the presence and crystalline degree of the perovskite structure, an adequate surface area, presence of α-oxygen and an easier formation of oxygen-deficient perovskite structures.

4. Conclusions

The effect of the RE cation and the calcination temperature, investigated on solid solutions of mixed perosvkites of formula $RECo_{0.50}Mn_{0.50}O_3$ (RE = La, Y, Er), show that $YCo_{0.50}Mn_{0.50}O_3$ forms a crystalline perovskite structure at low temperature (∼700 °C) with an adequate surface area and almost no changes in crystalline structure upon the calcination temperature (850 °C and 950 °C). For the $LaCo_{0.50}Mn_{0.50}O_3$ system, a less crystalline perovskite structure appears at 700 °C, increasing its crystallinity as the calcination temperature increases. For $ErCo_{0.50}Mn_{0.50}O_3$, which shows a higher surface area when calcined at 700 °C, its activity is the lowest due to the presence of segregated phases and a perovskite structure of low crystalline degree.

At the calcination temperatures of 850 °C and 950 °C, at which the surface area and crystalline degrees are almost the same for the La-, Y- and Er-systems, no differences in the catalytic activity were detected.

The catalytic activity in the methane combustion depends on the chemical composition and crystalline degree of the perovskite structure, a consequence of the calcination temperature. The RE cation which reaches the perovskite structure at lower temperature, that is, $YCo_{0.50}Mn_{0.50}O_3$, exhibits the highest catalytic activity.

In a separate work the magnetic properties of these perovskites will be studied, analyzed and discussed as a function of the calcination temperature and microstructure.

Acknowledgments

The authors thank Projects CNRS-CONICYT 22785 and 23910 and FONDECYT 1090018. C.M. Campos thanks BECAS-CHILE for a support for a one-year stay in Rennes, France. Authors are members of the Chilean-French Joint "Laboratory for Inorganic Functional Materials" LIA-MIF N° 836.

References

[1] C.N. Rao, B. Raveau (Eds.), Colossal Magnetoresistance Charge Ordering and Related Properties of Manganese Oxides, World Scientific, Singapore, 1998.
[2] Y. Tokura, Colossal Magnetoresistive Oxides, Gordon & Breach, New York, 2000.
[3] E.O. Wollan, W.C. Koehler, Phys. Rev. 100 (1955) 545.
[4] C. Moure, D. Gutierrez, O. Peña, P. Duran, J. Solid State Chem. 163 (2002) 377.
[5] C. Moure, D. Gutierrez, O. Peña, P. Duran, J. Am. Ceram. Soc. 86 (2003) 54.
[6] O. Peña, A.B. Antunes, G. Martinez, V. Gil, C. Moure, J. Magn. Magn. Mater. 310 (2007) 159.
[7] G. Blasse, J. Phys. Chem. Solids 26 (1965) 1969.
[8] N. Nishimori, K. Asai, M. Mizoguchi, J. Phys. Soc. Jpn. 64 (1995) 1326.
[9] G. Pecchi, C. Campos, O. Peña, L.E. Cadus, J. Mol. Catal. A: Chem. 282 (2008) 158.
[10] A.B. Antunes, V. Gil, C. Moure, O. Peña, J. Eur. Ceram. Soc. 27 (2007) 3927.
[11] L.A. Chick, L.R. Pederson, G.D. Maupin, J.L. Bates, Mater. Lett. 10 (1–2) (1990) 6.
[12] V. Goldschmidt, Skr. Nor. Viedenk. -Akad, Kl. I:Mater.-Naturvidensk.Kl. Nº. 8. 1926.
[13] E. Baran, Catal. Today 8 (1990) 133.
[14] S.K.S. Parashar, R.N.P. Choudhary, B.S. Murty, Ferroelectrics 325 (2005) 65.
[15] J. Petunchi, A. Lombardo, Catal. Today 8 (1990) 201.
[16] H. Provendier, C. Petit, C. Estournes, S. Libs, A. Kienemann, Appl. Catal. A 180 (1999) 163.
[17] L. Sis, G. Wirtz, J. Appl. Phys. 44 (1973) 12.
[18] J.L.G. Fierro, J. Tascón, L. Tejuca, J. Catal. 89 (1984) 206.
[19] M. Imamura, N. Matsubayashi, H. Shimada, J. Phys. Chem. B 104 (2000) 7348.
[20] N. Merino, B. Barbero, P. Grange, L. Cadús, J. Catal. 231 (2005) 232.
[21] B. Levasseur, S. Kaliaguine, Appl. Catal. B: Environ. 88 (2009) 305.
[22] H. Arai, T. Yamada, K. Eguchi, T. Seiyama, Appl. Catal. 26 (1986) 265.